ONLINE DATA SUPPLEMENT

SUPPLEMENTAL MATERIALS AND METHODS

METHODS

Generation of transgenic models.

The transgenic expression vector containing the 5.5-kb murine α-myosin heavy chain promoter generously provided by Dr. Jeffrey Robbins Children's Hospital Research Foundation, Cincinnati, OH. A PCR-amplified cDNA encoding rat cardiac TnI with Ser22 and Ser23 changed to Asp to mimic constitutive phosphorylation (cTnI$DD_{22,23}$ mice) or Ser22 changed to Ala and Ser23 changed to Asp residues to mimic partial dephosphorylation and Ser42 and Ser44 changed to Asp to mimic activation (cTnI $AD_{22,23}DD_{42,44}$ mice) was cloned into the *Sal*I site. Details of TG generation, breeding and genotyping have been previously described [1]. For experimental studies, the two TG mice models were compared with NTG littermates or age-matched C57BL/6 mice. All animal protocols were performed in accordance with institutional guidelines and approval of the IACUC.

Trabeculae isolation, force, sarcomeric length and $[Ca^{2+}]_i$ measurements

Male or female mice (6-9 months old) were anesthetized with pentobarbital (50mg/Kg^{-1}) and heparinized (100 U) intraperitoneally. Hearts were excised and perfused retrogradely ($\sim$15 ml/min) with dissecting Krebs–Henseleit (K-H) solution equilibrated with 95% O_2 and 5% CO_2. The dissecting K–H solution is composed of (in mM): NaCl 120, $NaHCO_3$ 20, KCl 5, MgCl 1.2, glucose 10, $CaCl_2$ 0.5, and 2,3-butanedione

monoximine (BDM) 20, pH 7.35–7.45 at room temperature (21–22 °C). Trabeculae from the right ventricle of the heart were dissected and mounted between a force transducer (Scientific Instruments, Heidelberg) and a motor arm. Force was expressed in millinewtons per square millimeter (mN/mm2) of cross-sectional area. Sarcomere length was adjusted as previously described [2], which correspond to resting sarcomeric lengths of 2.1-2.2 µm. The trabecula was then superfused with normal K–H solution (No BDM) at a rate of $\sim$ 10 ml/min and stimulated at 0.5 Hz for 30 minutes for stabilization. Dimensions of the muscles were measured with a calibration reticule in the ocular of the dissection microscope (× 40, resolution $\sim$ 10 µm). $[Ca^{2+}]_i$ was measured using the free acid form of fura-2 and absolute values calculated from in vivo calibrations described in our previous studies [3-5]. Briefly, Fura-2 potassium salt (Invitrogen) was microinjected iontophoretically into one cell and allowed to spread throughout the whole muscle (via gap junctions). Measurements were collected and digitalized through a data acquisition board (National Instruments). Custom written software (developed in LabVIEW) was used to analyze data on and off-line. Analyzed data were used to generate graphs in Origin 6.0, for clarity of illustrations, representative tracings of force twitch, Ca^{2+} transients and Force-$[Ca^{2+}]_i$ hysteresis loops were smoothed using adjacent averaging function (10 to 20 points).

Force-frequency relation in trabeculae

Muscles were kept at room temperature (21–22 °C), external $[Ca^{2+}]_o$ of 1.5mM and allowed to stabilized at 0.5Hz, then subjected to a stepwise increases on stimulation frequency (1 to 4 Hz) where developed force and $[Ca^{2+}]_i$ were recorded.

Off-line force-$[Ca^{2+}]_i$ hysteresis loops were used to identify $[Ca^{2+}]i$ at 50% of twitch activation ($ActECa_{50}$) and $[Ca^{2+}]i$ at 50% of relaxation ($RelECa_{50}$), to calculate slope steepness of activation and relaxation, individual segments between points B to C and C to A were dissected and fitted for linearity.

Isolated skinned fiber studies

Freshly isolated cardiac trabeculae were electrically stimulated (0.5Hz) and allowed to stabilize, then skinned by 5 to 10 min incubation in 1% Triton X-100 in relaxing solution (80 mM KCl, 25 mM HEPES, 10 mM K_2EGTA, 15 mM creatine phosphate sodium salt (Na_2CrP), 5 Na_2ATP, 5.15 mM $MgCl_2$, and 0.5 mM leupeptin). Varied Ca^{2+} concentrations $[Ca^{2+}]$ were achieved by mixing the relaxing solution and activating solution (10 mM Ca^{2+}-EGTA, 80 mM KCl, 25 mM HEPES, 15 mM Na_2CrP, 5 mM Na_2ATP, 4.75 mM $MgCl_2$, and 0.5 mM leupeptin, pH 7.2) in various ratios [6]. After reaching the highest calcium concentration trabecuale were washed in relaxing solution and incubated 1 hr in relaxing solution containing 30 U of catalytic subunit PKA (SIGMA). A new calcium activation protocol was carried out and $[Ca^{2+}]$ was calculated as previously described in detail [7]. Skinned steady-state force-$[Ca^{2+}]$ relationships were determined experimentally and fit to the Hill equation to yield F_{max}, or maximal Ca^{2+}-activated force, ECa_{50}, the $[Ca^{2+}]$ required for 50 % of maximal activation, and the Hill coefficient, as previously described [4].

Computational Methods.

Concerning specifically the dynamics of contraction, a six state model of the tropomyosyn interacting with troponin bound to Ca^{2+} has been taken into account [8, 9], see Model Scheme in Figure 8D. The Ca^{2+} transient drives the myofilament model. There is a feedforward loop in which Ca^{2+} binds to troponin during the transient and subsequent elicits the development of force by the myofilaments. A feedback loop also exists, because the affinity of troponin for Ca^{2+} is a function of developed force. Specifically the off-rate of Ca^{2+} binding from troponin is assumed to be a decreasing function of normalized force. Thus the level of developed force can alter the amount of Ca^{2+} bound to troponin and, subsequently, alter the activator Ca^{2+} transient. The set of equations accounting for force generation in relation to Ca^{2+} dynamics in the ECME model are provided in the Appendix I. A more detailed description of the model was presented elsewhere [8] .

ECME model

The integrated model (ECME) has been built in a modular way by assembling the expressions representing each of the processes taken into account. The code of the integrated ECME model, written in C^{++}, contains 50 ordinary differential equations (ODEs) in Microsoft Visual Studio environment (Microsoft Corporation, Redmond, WA). Equations were integrated numerically using CVODE, a stiff ODEs solver in C, developed by Cohen and Hindmarsh, that uses variable-coefficient Adams and BDF methods, (http://citeseer.ist.psu.edu/1230.html).The source code of the ECME model is available for download from;

http://senselab.med.yale.edu/ModelDB/ShowModel.asp?model=105383

To run the Force-Ca^{2+} steady-state simulations, we assembled the force related equations together with Ca^{2+} buffering by troponin with a MatCont package that runs on a MATLAB environment (MatCont 2.4, [10]), for more detailed information about MatCont visit

http:// www.matcont.ugent.be/matcont.html).

Force-$[Ca^{2+}]_i$ dynamic loops simulated with the integrated ECME model.

Computer simulations were run at 2 Hz of stimulation, which is the highest frequency attained in this model. After the solutions of ODEs (ordinary differential equations) reach a pseudo steady-state in the state variables under each parametric condition, this is usually 500 s from the common initial condition, developed force and calcium were recorded and expressed in mN/mm^2 and µM, as described previously [8]. To compare genotype outcome see Figure 8A,a) and to compare genotype specific parametric conditions see Table 5.

ECME model simulations of force frequency relationship (FFR).

The integrated ECME computational model was run at a range of frequencies (0.5, 1.0, 1.5 and 2.0). Each genotype was run under the same set of parametric conditions indicated in Table 5. Simulation was run until a pseudo steady-state was reached (i.e a state in which the position and the amplitude of cycling for each state variable is constant in time). Then, five to ten cycles were simulated and their maximal and minimal values of Ca^{2+} and force transients were recorded. The difference between maximum and minimum renders the amplitude of the twitch force developed, that was recorded for

each frequency and expressed as mN/mm^2. Genotype corresponding to each curve is as indicated in Figure 8A, c).

Computer simulation of Force-Ca^{2+} steady-state relationships.

The MatCont package was used to create a model containing just the force and Ca^{2+} buffering modules (see above description of Computational Methods). The model was run until a steady state was attained and from that point bifurcation analysis was performed with Ca^{2+} as bifurcation parameter. The steady state Force-Ca^{2+} relations (not shown) displayed the following EC_{50} values, for NTG (EC_{50}= 0.46) and for cTnIDD$_{22,23}$ (EC_{50}=0.49 μM), whereas the simulations of the cTnI AD$_{22,23}$DD$_{42,44}$, exhibit a larger EC_{50} (0.56 μM). The simulation data were quantitatively smaller than in the experimental data but the rightward shift when compared to NTG were similar.

Force-[Ca^{2+}]*i* loops analysis of EC_{50} and slopes steepness in activation and relaxation segments.

Measurements for force and calcium signals were collected and digitalized through a data acquisition board (National Instruments). Custom written software (developed in LabVIEW) was used to analyze data on-line and off-line. Data analyzed off-line provided normalized force values (0 to 1) and absolute [Ca^{2+}]*i* μM/L in a hysteresis loop averaging 5 twitch cycles. Here the mid-point (0.5) of segment B to C on Y-axis was taken and correspondent value of X-axis [Ca^{2+}]*i* was considered as EC_{50} of activation (ActEC_{50}), the same quantification approach was taken to identify mid-point of C to A

segment ($RelEC_{50}$). LabVIEW force and calcium data were exported and analyzed in Origin 6.0. Force-Ca^{2+} hysteresis loops were smoothed using adjacent averaging function (10 to 20 points). Here, slopes of activation and relaxation were calculated dissecting individual segments (B to C and C to A) and fitting them for linearity, r values for activation fell between -0.90 to -0.99 ($p < 0.0001$), whereas for relaxation r values fell between 0.90 to 0.99 ($p < 0.0001$). EC_{50} and slope steepness was group averaged (*n*= 3-5) and compared. Graphs and statistical analyses were performed with GraphPad 5.0, using two-way ANOVA.

Immunoblots

Protein was isolated from liquid nitrogen flash-frozen hearts (n=3-5). Hearts were thawed in a cold isolation buffer containing (50mM $NaCl_2$, 5mM EDTA, 1% SDS) and proteinase inhibitor cocktail (Mini-EDTA free, Roche) and phosphatase inhibitor cocktail (PhosSTOP, Roche) and homogenized using a tissue homogenizer (OmniTH). Samples were incubated at 4°C for 30 minutes, centrifuges at 14,000g for 15 minutes at 4°C and supernatants were recovered. Protein samples were quantified in triplicate using Bio-Rad DC assay (Bio-Rad). Samples (10 µg total protein/lane) were separated by 4-12% Bis-Tris SDS gel electrophoresis (Invitrogen) under reducing conditions. Proteins were transferred to nylon membranes (Invitrogen) and blocked for 1 hour with 1X Blocking Reagent (Roche) diluted in Tris-buffered saline + 0.05% Tween20 (TBS-T). PLB, phospho PLB, SERCA2a, NCX were detected using mouse anti-PLB (1:500, ABR), rabbit anti-phosphoSer16 PLB (1:500, Cell Signaling), mouse anti-SERCA2a (1:1000, ABR), mouse anti-NCX (1:1000, ABR) incubated overnight at 4°C in 1X Blocking

Reagent (Roche) diluted in TBS-T. Following washes with TBS-T membranes were incubated with an HRP-conjugated goat anti-mouse antibody (1:10,000, Santa Cruz) or goat anti-rabbit (1:10,000, Pierce) bands were detected by ECL (Amersham GE) or WestPico (Pierce) using BioMax Films (Kodak). Membranes were stripped (Restore, Pierce) and incubated with various antibodies for respective loading controls anti-desmin (Sigma), anti-actin (Sigma), anti-tubulin (Abcam), anti-calsequestrin (ABR) and immunoreactive bands detected as above. All signals were within linear range and the densitometric analyses were performed using NIH ImageJ Software and ratios of integrated density calculated in arbitrary units (A.U.).

Myofilament Phosphorylation Levels.

Hearts were excised and perfused retrogradely (~15 ml/min) with dissecting Krebs–Henseleit (K-H) as described the methods section, trabeculae from the right ventricle of the heart were dissected in less than 10 minutes, then remaining heart tissue was soaked on ice cold relaxing buffer (KCl 75mM, Imidazole 10mM, pH 7.0, $MgCl_2$ 2mM, EGTA 2mM, PhosphoCreatine 40mM, 2,3-butanedione monoximine (BDM) 50mM, DTT 1mM, Benzamidine-HCL 1mM, Triton X-100 1%, PhosStop 1X, Mini-EDTA free 1X in water HPLC grade), minced and myofilament proteins were immediately isolated as previously described [11], all solutions contained PhosStop (Roche) and proteinase inhibitor cocktail (Mini-EDTA free, Roche). Myofilament preparations were kept at -80ºC until further use. On the day of experiment preparations were thaw on ice, sonicated in 300 µl of 100 mM Tris (pH 8.0), 2% SDS and centrifuged at 16,000 x g for 15 minutes. Protein concentrations were performed using the Bio-Rad DC assay (Bio-Rad), 5µg of

myofilament extracts were separated by SDS-PAGE (4-12% NuPage Bis-Tris, Invitrogen) gel electrophoresis using MES running buffer. To determine global phosphorylation of myofilament proteins, a phosphoprotein gel staining (Pro-Q® Diamond, Invitrogen) was used as per manufacturer's instruction, following the long protocol version. Briefly, protein gels were fixed (50% (v/v) Methanol, 10%(v/v) acetic acid) O/N at RT, followed by one wash in HPLC grade water, incubation with Pro-Q® Diamond (Invitrogen) for 90 min, washed in HPLC water, incubated 90 minutes in de-staining solution (20%(v/v) acetonitrile, 50mM sodium acetate (pH 4.0) and washed again in HPLC water for 5 minutes. Gels were scanned using Typhoon 9400 (GE Healthcare) with 533 nm Excitation/560 LP filter at 100 microns, PMT voltages were adjusted to ensure that signal intensity was within linear range. In order to confirm the specificity of the method for phosphorylated proteins, 1 µl of PeppermintStick™ phosphoprotein molecular weight standards were included. Total protein bands were visualized by incubating gels in Sypro® Ruby gel stain solution overnight at room temperature and destaining with 10% (v/v) methanol, 7% (v/v) acetic acid. Total protein bands were imaged as described for the phosphostain. Band densitometry analysis was calculated using ImageQuantTL v2005 (GE Health Care).

SUPPLEMENTAL RESULTS & DISCUSSION

Myofilament Feedback onto Calcium Handling

Immunoblotting studies were performed in NTG, cTnIDD$_{22,23}$ and cTnIAD$_{22,23}$DD$_{42,44}$ (*n*=3-5) mice to establish the basal status of several calcium handling proteins (PLB,

pPLB-Ser16, SERCA2a and NCX) and their possible contribution to the differences observed in these lines. Whole heart homogenates were analyzed for total phospholamban levels normalized to Desmin, phosphorylated PLB normalized to total PLB, SERCA2a normalized to tubulin, and NCX normalized to calsequestrin, supplemental Figure1A-D, respectively. Protein homogenates from cTnIDD$_{22,23}$ mice showed a 30.2±1.53% increase in total PLB content than NTG mice ($p<0.05$). In contrast, normalized phosphorylated PLB, SERCA2a and NCX protein expression levels were comparable to those in NTG mice. On the other hand, cTnIAD$_{22,23}$DD$_{42,44}$ mice displayed a 56.7±7.4% reduction in phosphorylated PLB when compared to NTG ($p<0.05$). Different from what we had noted earlier [7], we did not find decreased SERCA2a levels. However, in this study we used cardiac tissue from the exact mice used for physiologic studies, whereas in the Bilchick studies stored samples were used from mice not used for physiological studies, and in addition used a different loading control (α-tubulin instead of α-actin). It is possible those factors might have accounted to the difference in the findings.

The content of Ca^{2+} handling proteins might partially explain the features noted in Ca^{2+} transients kinetics. In cTnIDD$_{22,23}$ mice we found a modest increase in total PLB content accompanied with normal PLB phosphorylation levels, thus no changes in SERCA2a pump inhibition were expected. In agreement with this result, Ca^{2+} transient kinetics were not affected at baseline or at higher frequencies. On the other hand, cTnIAD$_{22,23}$DD$_{42,44}$ mice showed a depressed Ser16-PLB phosphorylation without compensatory increase in expression of SERCA2a. The latter finding correlates with

what has been reported for human heart failure [12]. It is generally accepted that this alteration is expected to inhibit SERCA2a pump activity, resulting in impaired Ca^{2+} transient and twitch kinetics [12, 13]. In addition, we observed that the cTnIA$D_{22,23}$D$D_{42,44}$ mice had a subtle although not significant decrease of NCX levels, however, it is known that in rodents NCX is a small contributor to Ca^{2+} dynamics compared to human heart [14].

We reason that in our study these changes might reflect chronic adaptations to the alterations introduced to the myofilament apparatus. Although SERCA2a levels were not altered in cTnIA$D_{22,23}$D$D_{42,44}$ at baseline decreased pPLB levels were enough to compromise the Ca^{2+} transient kinetics of decay (RT50%) and twitch relaxation rates (RT75%) at higher frequencies (Figures 3D and Figure 4A, respectively).

Phosphorylation of other myofilament proteins are not altered in these models.

We determined the phosphorylation pattern (Pro-Q Diamond) of myofilament preparations. Their results were normalized to total protein content (Sypro Ruby) and compared between NTG, cTnIDD$_{22,23}$ and cTnIA$D_{22,23}$D$D_{42,44}$ (*n*=3) mice. Our results show that at basal conditions phosphorylation status of myofilament proteins other than TnI were not significantly changed between NTG and cTnIDD$_{22,23}$ and cTnIA$D_{22,23}$D$D_{42,44}$, see supplemental Figure2. However, cTnI in the cTnIDD$_{22,23}$ mutant mice had a decreased ProQ signal. We attribute this change to the nearly complete replacement of the native TnI with the mutant. Since the PKA sites account for most of the native phosphorylation of TnI stoichiometrically, the change from Ser to Asp in these sites likely decreases the affinity of ProQ dye for the mutated TnI protein. The

cTnIA$D_{22,23}$$DD_{42,44}$ contain a partial replacement and have been previously demonstrated to have equal staining to NTG mice with a PKA site specific antibody [7]. It is also worth noting that phosphorylation levels of TnT were also unchanged in this analysis, in agreement with 2D gels reported by Bilchick and colleagues [7].

References

[1] Murphy AM, Kogler H, Georgakopoulos D, McDonough JL, Kass DA, Van Eyk JE, et al. Transgenic mouse model of stunned myocardium. Science. 2000 Jan 21; 287(5452): 488-91.

[2] Gao WD, Liu Y, Mellgren R, Marban E. Intrinsic myofilament alterations underlying the decreased contractility of stunned myocardium. A consequence of Ca2+-dependent proteolysis? Circ Res. 1996 Mar; 78(3): 455-65.

[3] Backx PH, Gao WD, Azan-Backx MD, Marban E. The relationship between contractile force and intracellular [Ca2+] in intact rat cardiac trabeculae. J Gen Physiol. 1995 Jan; 105(1): 1-19.

[4] Gao WD, Backx PH, Azan-Backx M, Marban E. Myofilament Ca2+ sensitivity in intact versus skinned rat ventricular muscle. Circ Res. 1994 Mar; 74(3): 408-15.

[5] Gao WD, Perez NG, Marban E. Calcium cycling and contractile activation in intact mouse cardiac muscle. J Physiol. 1998 Feb 15; 507 (Pt 1): 175-84.

[6] Fabiato A. Myoplasmic free calcium concentration reached during the twitch of an intact isolated cardiac cell and during calcium-induced release of calcium from the sarcoplasmic reticulum of a skinned cardiac cell from the adult rat or rabbit ventricle. J Gen Physiol. 1981 Nov; 78(5): 457-97.

[7] Bilchick KC, Duncan JG, Ravi R, Takimoto E, Champion HC, Gao WD, et al. Heart failure-associated alterations in troponin I phosphorylation impair ventricular relaxation-afterload and force-frequency responses and systolic function. Am J Physiol Heart Circ Physiol. 2007 Jan; 292(1): H318-25.

[8] Cortassa S, Aon MA, O'Rourke B, Jacques R, Tseng HJ, Marban E, et al. A computational model integrating electrophysiology, contraction, and mitochondrial bioenergetics in the ventricular myocyte. Biophys J. 2006 Aug 15; 91(4): 1564-89.

[9] Rice JJ, Winslow RL and Hunter WC. Comparison of putative cooperative mechanisms in cardiac muscle: length dependence and dynamic responses. Am. J. Physiol. 276 (Heart Circ. Physiol. 45) 1999: H1734–H1754.

[10] Dhooge A, Govaerts W, Kuznetsov YA, Meijer HGE, Sautois B. New features of the software MatCont for bifurcation analysis of dynamical systems. London: Taylor & Francis Group 2008:147-75.

[11] Murphy AM, Solaro RJ. Developmental difference in the stimulation of cardiac myofibrillar Mg2(+)-ATPase activity by calmidazolium. Pediatr Res. 1990 Jul; 28(1): 46-9.

[12] Schwinger RH, Munch G, Bolck B, Karczewski P, Krause EG, Erdmann E. Reduced Ca(2+)-sensitivity of SERCA 2a in failing human myocardium due to reduced serin-16 phospholamban phosphorylation. J Mol Cell Cardiol. 1999 Mar; 31(3): 479-91.

[13] Brixius K, Wollmer A, Bolck B, Mehlhorn U, Schwinger RH. Ser16-, but not Thr17-phosphorylation of phospholamban influences frequency-dependent force generation in human myocardium. Pflugers Arch. 2003 Nov; 447(2): 150-7.

[14] Bers DM. Cardiac excitation-contraction coupling. Nature. 2002 Jan 10; 415(6868): 198-205.

Supplemental Figure Legends

Supplemental Figure 1. Immunoblots of Calcium Handling proteins from NTG and cTnIDD$_{22,23}$, cTnIAD$_{22,23}$DD$_{42,44}$ transgenic models. A, Immunoblot of phospholamban (PLB) normalized with Anti-desmin showing an increase of 30.2±1.53% in total PLB content in cTnIDD$_{22,23}$ when compared to NTG. **B**, Immunoblot of phosphorylated phospholamban (pPLB) normalized to total levels of phospholamban (PLB) showing a reduction of 56.7±7.4% in pPLB levels in cTnIAD$_{22,23}$DD$_{42,44}$ when compared to NTG. **C,** Immunoblot of sarco(endo)plasmic reticulum Ca^{2+} ATPase (SERCA2a) normalized with tubulin showed no differences between groups. **D,** Immunoblot of Na^{2+}-Ca^{2+} Exchanger (NCX) normalized with Anti-calsequestrin (CSQ) showing a non significant decrease in NCX levels when compared to NTG. One membrane was used for one target protein and their respective loading control. Films were scanned and integrated density was calculated with NIH ImageJ software, quantitative data means ± s.e.m from *n*= 3-5 are represented in the graphs (*p < 0.05).

Supplemental Figure2. Myofilament phosphorylation levels. Phosphorylation of myofilament preparations were determined by Pro-Q Staining and normalized to total content (Sypro Ruby) from NTG, cTnIDD$_{22,23}$ and cTnIAD$_{22,23}$DD$_{42,44}$. **A**, Shows representative SDS-PAGE SyproRuby staining fluorescent counts profile analysis on y axis, molecular weight markers on x axis with, TnI migration is highlighted by a dashed

box. **B**, Corresponding Pro-Q staining profile analysis **C**, Comparison of normalized phosphorylation leves expressed as ratio of ProQ/Sypro Ruby signals, note that cTnI phosphorylaton is significantly reduced in $cTnIDD_{22,23}$ (*p<0.05).

Supplemental Figure 3. Diastolic $[Ca^{2+}]_i$ levels during Force-Frequency Response. Shows averaged $[Ca^{2+}]_i$ diastolic levels at various stimulation frequencies (1, 2, 3 and 4 Hz) from NTG (*n*=5), $cTnIDD_{22,23}$ (*n*=4) and $cTnIAD_{22,23}DD_{42,44}$ (*n*=6) mice. Similar to systolic Ca^{2+} transients, $[Ca^{2+}]_i$ diastolic levels from all three mice groups increased with frequency (*p < 0.05 one-way ANOVA). However, genotype did not showed an overall effect when all groups were compared (p= ns by two-way RM ANOVA). All data are expressed as means± s.e.m.

Table 1. Developed Force versus Frequency. Two-way Repeated Measures ANOVA with post-hoc (Bonferroni's pos-test)

Frequency	NTG (n=8)	$cTnIDD_{22,23}$ (n=7)		$cTnIAD_{22,23}DD_{42,44}$ (n=7)	
	ave ± s.e.m.	ave ± s.e.m.	p value *vs* NTG	ave ± s.em	p value *vs* NTG
1 Hz	6.11 ± 1.94	5.08 ± 1.40	n.s.	4.23 ± 2.95	n.s.
2 Hz	16.60 ± 4.51	11.99 ± 3.09	n.s	4.21 ± 1.30	n.s
3 Hz	23.43 ± 6.56	17.01 ± 3.63	n.s	5.85 ± 1.99	$p<0.01$
4 Hz	19.72 ± 4.55	14.46 ± 2.17	n.s	6.29 ± 2.25	n.s

Expressed units are mN/mm^2

Table 2. $[Ca^{2+}]_i$ –versus Frequency. Two-way Repeated Measures ANOVA with post-hoc (Bonferroni's pos-test).

Frequency	NTG (n=5)	$cTnIDD_{22,23}$ (n=4)		$cTnIAD_{22,23}DD_{42,44}$ (n=6)	
	ave ± s.e.m.	ave ± s.e.m.	p value *vs* NTG	ave ± s.em	p value *vs* NTG
1 Hz	0.50 ± 0.20	0.13 ± 0.02	n.s	0.32 ± 0.08	n.s
2 Hz	1.03 ± 0.18	0.36 ± 0.06	p<0.05	0.84 ± 0.26	n.s
3 Hz	1.42± 0.19	0.56 ± 0.13	p<0.05	1.17 ± 0.27	n.s
4 Hz	1.93 ± 0.33	0.64 ± 0.17	p<0.01	1.29 ± 0.29	n.s

Expressed units are µM/L

Table 3. Factors affecting Force Frequency Relationship and Twitch Kinetics.

Overall effects by Two-way Repeated Measures ANOVA.

	FFR	RT50%.	RT75%	RT90%	TTP
Interaction	Yes*	No	No	No	No
Frequency	Yes***	Yes***	Yes***	Yes***	Yes***
Genotype	Yes*	No	Yes*	BL p=0.057	Yes*
Matching	Yes	Yes***	Yes*	No	Yes***

*p < 0.05

***p <0.0001

BL= border line

Matching refers to paired or matched subjects

When matching was not possible non repeated measures two-way ANOVA was performed

Table 4. Factors affecting $[Ca^{2+}]_i$ -Frequency Relationship and $[Ca^{2+}]_i$ Kinetics.

Overall effects by Two-way Repeated Measures ANOVA

	$[Ca^{2+}]_i$ -FR.	RT50%.	RT75%	RT90%	TTP
Interaction	No	No	No	No	No
Frequency	Yes***	Yes***	Yes***	Yes***	No
Genotype	Yes*	Yes*	No	No	Yes*
Matching	Yes***	Yes***	Yes****	No	Yes*

*p < 0.05

***p <0.0001

Matching refers to paired or matched subjects

When matching was not possible non repeated measures two-way ANOVA was performed

Table 5. Summary of parameters employed in ECME computational model. Systematic simulations of force production and calcium buffering found this set of parameters to closely correlate with experimental behavior.

Genotype	High affinity association khtrpn (+)	High affinity dissociation khtrpn (-)	Low affinity association khtrpn (+)	Low affinity dissociation khtrpn (-)
NTG	1000 mM^{-1} ms^{-1}	0.00011 mM^{-1} ms^{-1}	100 mM^{-1} ms^{-1}	0.08 mM^{-1} ms^{-1}
$cTnIDD_{22,23}$	50 mM^{-1} ms^{-1}	0.00099 mM^{-1} ms^{-1}	400 mM^{-1} ms^{-1}	0.24 mM^{-1} ms^{-1}
$cTnIAD_{22,23}DD_{42,44}$	50 mM^{-1} ms^{-1}	0.00099 mM^{-1} ms^{-1}	100 mM^{-1} ms^{-1}	0.24 mM^{-1} ms^{-1}

Appendix I:

Equations related to Ca^{2+} buffering in myofibrils

$$J_{trpn} = \frac{d[HTRPNCa]}{dt} + \frac{d[LTRPNCa]}{dt}$$	A81
$$\frac{d[HTRPNCa]}{dt} = k_{htrpn}^{+} [Ca^{2+}]_i \left([HTRPN]_{tot} - [HTRPNCa]\right) - k_{htrpn}^{-} [HTRPNCa]$$	A87
$$\frac{d[LTRPNCa]}{dt} = k_{ltrpn}^{+} [Ca^{2+}]_i \left([LTRPN]_{tot} - [LTRPNCa]\right) - k_{ltrpn}^{-} \left(1 - \frac{2}{3} Force_{Norm}\right) [LTRPNCa]$$	A88

Force generation model

$$\frac{d[P_o]}{dt} = -\left(k_{pn}^{trop} + f_{01}\right)[P_o] + k_{np}^{trop} [N_0] + g_{01}(SL)\,[P_1]$$	A96
$$\frac{d[P_1]}{dt} = -\left(k_{pn}^{trop} + f_{12} + g_{01}(SL)\right)[P_1] + k_{np}^{trop} [N_1] + f_{01}\,[P_0] + g_{12}(SL)\,[P_2]$$	A97
$$\frac{d[P_2]}{dt} = -\left(f_{23} + g_{12}(SL)\right)[P_2] + f_{12}\,[P_1] + g_{23}(SL)\,[P_3]$$	A98

$$\frac{d[P_3]}{dt} = -\, g_{23(SL)}[P_3] + f_{23}[P_2]$$	A99
$$\frac{d[N_1]}{dt} = k_{pn}^{trop}[P_1] + \left(k_{np}^{trop} + g_{01}^{'}(SL)\right)[N_1]$$	A100
$$[N_0] = 1 - \left([N_1] + [P_0] + [P_1] + [P_2] + [P_3]\right)$$	A101
$$f_{01} = 3 \times f_{XB}$$	A102
$$f_{12} = 10 \times f_{XB}$$	A103
$$f_{23} = 7 \times f_{XB}$$	A104
$$g_{01} = 1 \times g_{XB}^{min}$$	A105
$$g_{12} = 2 \times g_{XB}^{min}$$	A106
$$g_{23} = 3 \times g_{XB}^{min}$$	A107
$$g_{01}(SL) = 1 \times \phi \times g_{XB}^{min}$$	A108
$$g_{12}(SL) = 2 \times \phi \times g_{XB}^{min}$$	A109
$$g_{23}(SL) = 3 \times \phi \times g_{XB}^{min}$$	A110

$$\phi = 1 + \frac{2.3 - SL}{(2.3 - 1.7)^{1.6}}$$	A111
$$k_{np}^{trop} = k_{pn}^{trop} \left[\frac{[LTRPNCa]}{K_{1/2}^{trop} \; [LTRPN]_{tot}} \right]^{N^{trop}}$$	A112
$$K_{1/2}^{trop} = \left(1 + \frac{K_{Ca}^{trop}}{1.7 \; 10^{-3} - 0.8 \; 10^{-3} \; \frac{(SL - 1.7)}{0.6}} \right)^{-1}$$	A113
$$N^{trop} = 3.5 \times SL - 2.0$$	A114
$$K_{Ca}^{trop} = \frac{k_{ltrpn}^{-}}{k_{ltrpn}^{+}}$$	A115
$$\sum PATHS = g_{01} \; g_{12} \; g_{23} + f_{01} \; g_{12} \; g_{23} + f_{01} \; f_{12} \; g_{23} + f_{01} \; f_{12} \; f_{23}$$	A116
$$P1_{max} = \frac{f_{01} \; g_{12} \; g_{23}}{\sum PATHS}$$	A117
$$P2_{max} = \frac{f_{01} \; f_{12} \; g_{23}}{\sum PATHS}$$	A118
$$P3_{max} = \frac{f_{01} \; f_{12} \; f_{23}}{\sum PATHS}$$	A119

$$\text{Force} = \zeta \frac{P_1 + N_1 + 2\,P_2 + 3\,P_3}{P1_{max} + 2\,P2_{max} + 3\,P3_{max}}$$	A120
$$\text{Force}_{Norm} = \frac{P_1 + N_1 + P_2 + P_3}{P1_{max} + P2_{max} + P3_{max}}$$	A121

Apendix I. Describes the equations related to force generation and Ca^{2+} buffering, their numbering correspond to the order in original source [8]. For additional details and the complete ECME model description see [8].

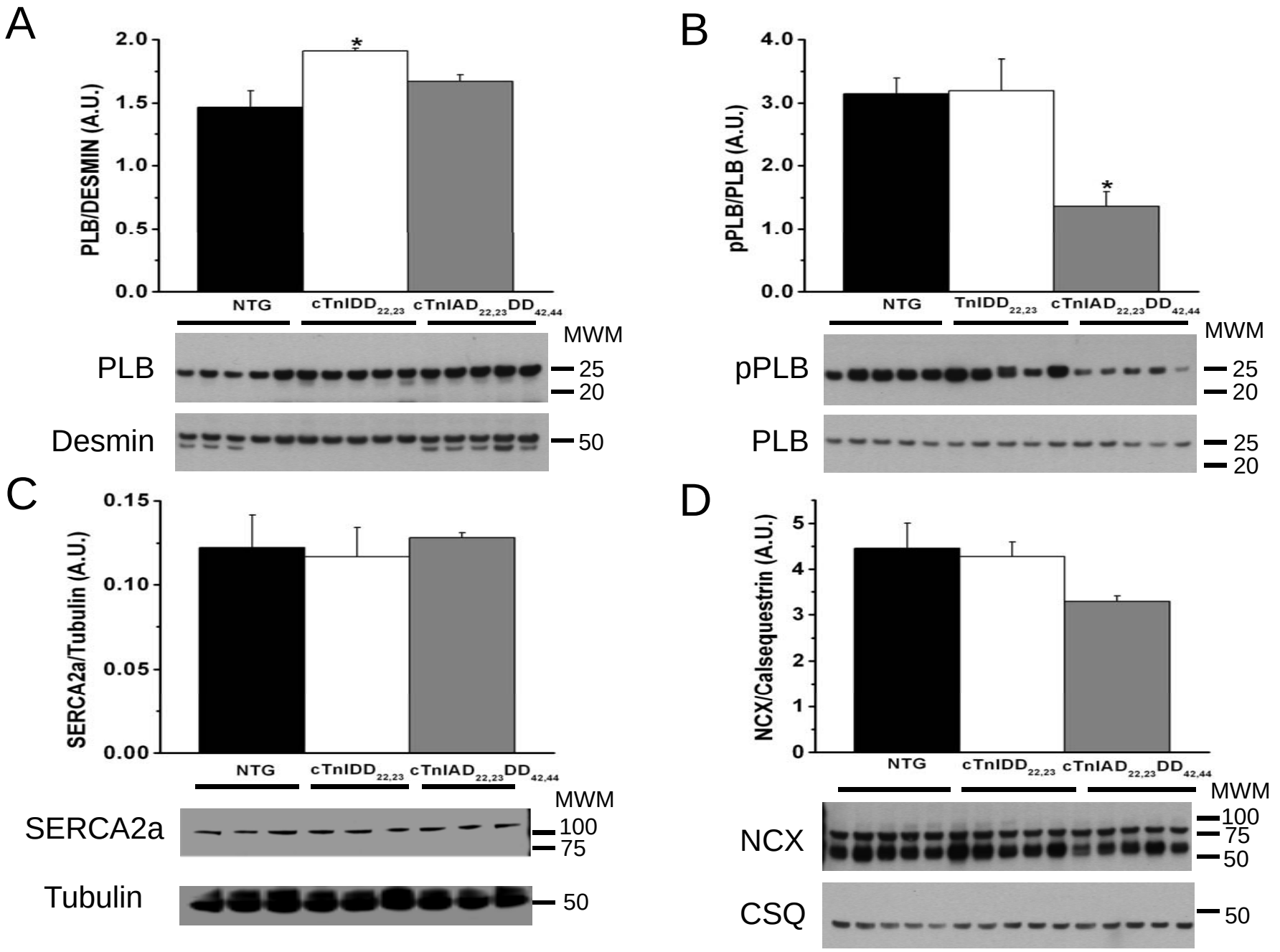

Supplemental Figure 1

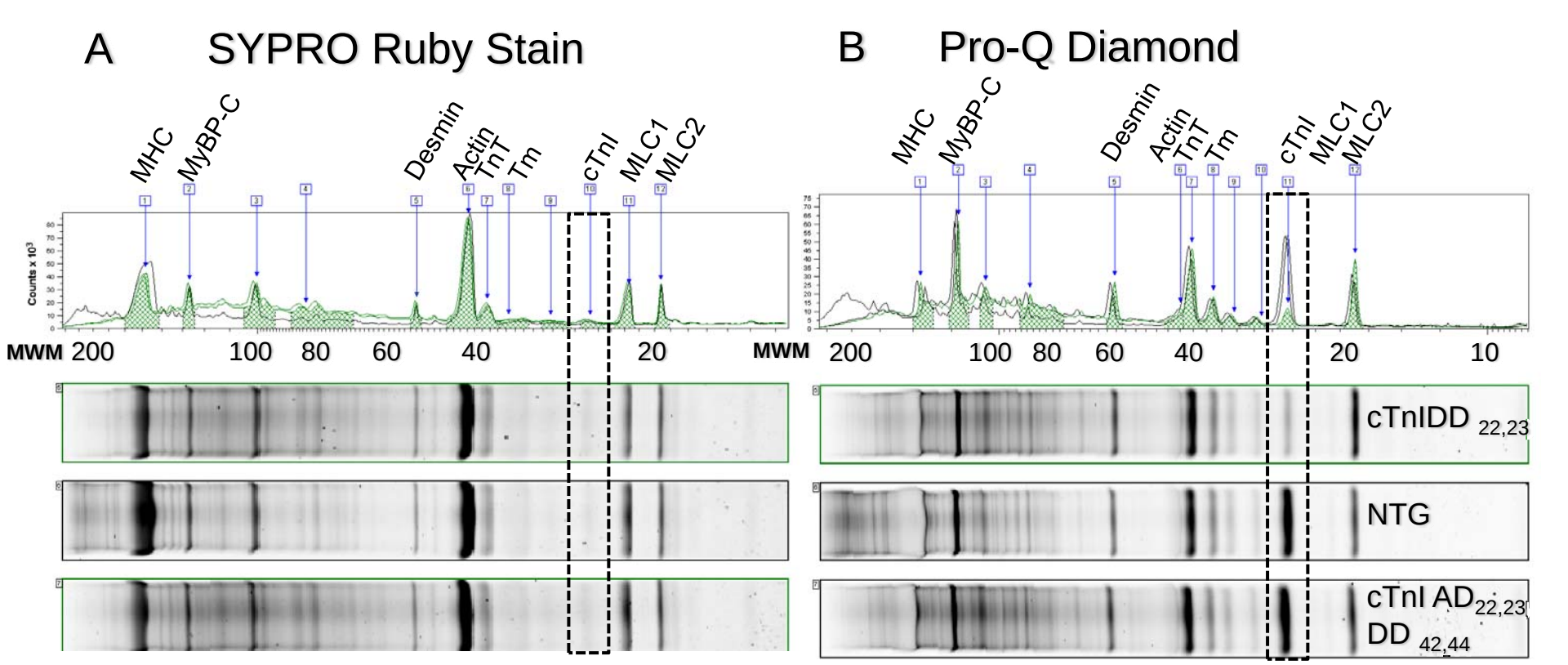

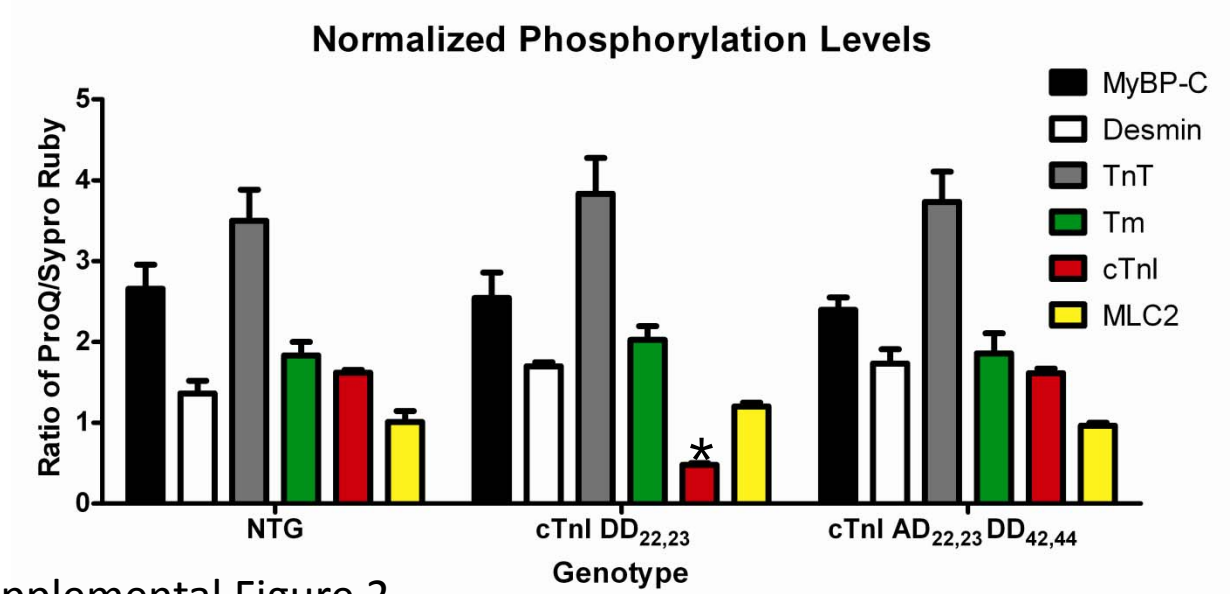

Supplemental Figure 2

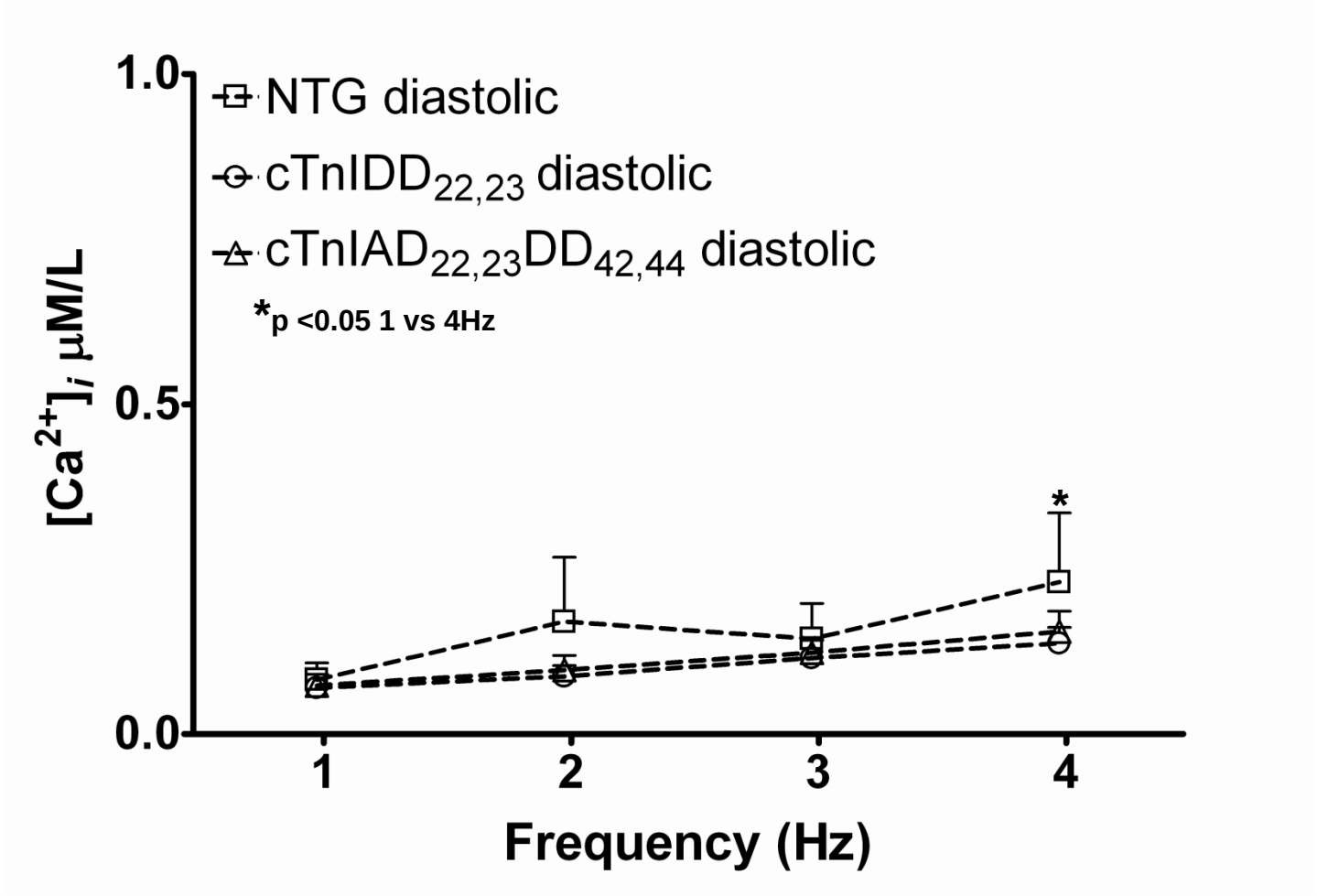

Supplemental Figure 3